Supplemental Material

On-chip terahertz metasensor for quantitative multi-component biomolecular identification

Xitan Xu[1], Haoyu Duan[1], Yao Lu[1, *], Yuchen Zhang[2], Ziyang Zheng[1], Baohua Jia[3, **], Qiang Wu[1, 4, ***], and Jingjun Xu[1, 4]

[1] Key Laboratory of Weak-Light Nonlinear Photonics, Ministry of Education, TEDA Institute of Applied Physics and School of Physics, Nankai University, Tianjin 300457, China
[2] School of Science, Tianjin Chengjian University, Tianjin 300384, China
[3] Centre for Atomaterials and Nanomanufacturing (CAN), School of Science, RMIT University, Melbourne, Victoria 3000, Australia
[4] Collaborative Innovation Center of Extreme Optics, Shanxi University, Taiyuan, Shanxi 030006, China
* yaolu@nankai.edu.cn
** baohua.jia@rmit.edu.au
*** wuqiang@nankai.edu.cn

1. Time-resolved phase-contrast imaging system.

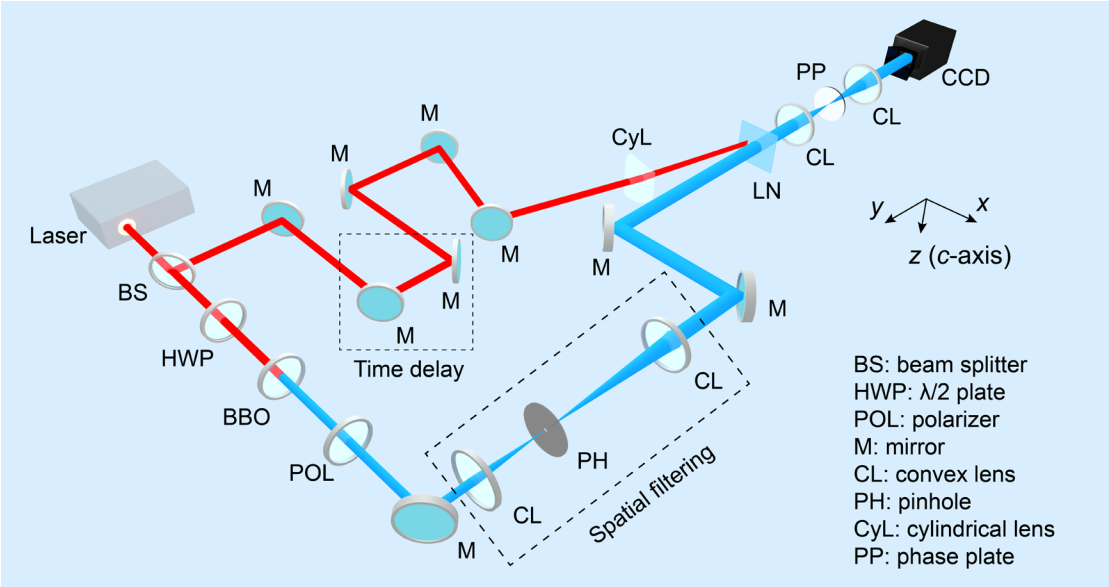

Figure S1 Schematic of the experimental setup of the time-resolved phase-contrast imaging system.

Figure S1 shows the schematic of the experimental setup of the time-resolved phase contrast imaging system. The femtosecond laser pulse (800 nm central wavelength, 1 kHz repetition rate, 80 fs width) from a Ti: Sapphire regenerative

amplifier is split into two beams by a 90:10 (reflection: transmission) beam splitter. The reflected beam with higher energy is used as the pump beam, which is normally incident to a time delay line and focused on the LN wafer though a 10-cm focal-length cylindrical lens to generate THz waves. The transmitted beam with lower energy is used as the probe beam to irradiate the LN wafer after frequency doubling, spatial filtering and beam expansion.

During the propagation in the LN wafer, the THz wave will cause a change in refractive index $\Delta n(x,z)$ of the medium due to the electro-optical effect, and introduce a phase shift after the probe beam though the LN wafer[1]:

$$\Delta\varphi(x,z) = 2\pi\frac{h}{\lambda_{\text{probe}}}\Delta n(x,z) = 2\pi\frac{h}{\lambda_{\text{probe}}}\frac{n_{\text{eo}}^3 r_{33}}{2}E_z(x,z), \tag{S1}$$

where h is the thickness of the LN wafer, λ_{probe} stands the probe beam wavelength, n_{eo} and r_{33} denote the extraordinary refractive index and the electro-optic coefficient of the LN at the probe wavelength of 400 nm, respectively. E_z represents the electric field signal of the THz wave. The phase shift $\Delta\varphi(x,z)$ of the probe beam can be converted into the intensity information $I(x,z)$ through the phase contrast technique based on a 4f system, and then can be collected by a CCD camera:

$$\begin{aligned} I(x,z) &= I_0(x,z)\{3 - 2[\cos\Delta\varphi(x,z) + \sin\Delta\varphi(x,z)] \\ &\approx I_0(x,z)[1 - 2\Delta\varphi(x,z)], \end{aligned} \tag{S2}$$

where $I_0(x,z)$ represents the intensity of the probe beam without the THz wave. Consequently, based on Eqs. S1 and S2, the spatial distribution of the THz wave can be retrieved from the intensity change of the probe beam:

$$E_z(x,z) = -\frac{\lambda_{\text{probe}}}{2\pi h n_{\text{eo}} r_{33}}\frac{\Delta I(x,z)}{I_0(x,z)}, \tag{S3}$$

with $\Delta I(x,z) = I(x,z) - I_0(x,z)$. By changing the time delay between the pump and probe beams with a time delay line and repeating above data acquisition, the complete spatiotemporal evolution data $E_z(x,z,t)$ of the THz wave in the LN wafer can be obtained.

2. Theoretical calculation of SW mode and SSPP mode

When the THz wave propagates in the subwavelength thick LN wafer, its

propagation mode is significantly modulated by the structure of the planar subwavelength waveguide (SW). In the previous work, we have introduced a general solution to the LN SW with air claddings systematically[2]. For the fundamental mode of transverse electric (TE) mode propagating along the *x*-axis, the eigenmode equation can be simplified to:

$$\kappa h = 2\tan^{-1}\left(\frac{p_0}{\kappa}\right), \tag{S4}$$

here, $\kappa = \sqrt{k_0^2 n_e^2 - k_{SW}^2}$, $p_0 = \sqrt{k_{SW}^2 - k_0^2 n_0^2}$, k_0 represents the wavevector in the free space, h is the thickness of the LN wafer, n_e and n_e denote the refractive index of the air and LN crystals.

Figure S2 plots the dispersion curve of the THz wave of the SW mode in the 20 μm thick LN wafer, which can be obtained from Eq. S4. The effective refractive index can be calculated by:

$$n_{eff}(f) = \frac{ck_{SW}}{2\pi f}, \tag{S5}$$

At the interface between the metasurface array and the LN wafer, the dispersion curve of the SSPP mode can be obtained from Eq. S6[3]:

$$k_{SSPP} = \frac{2\pi f}{c}\sqrt{\frac{\varepsilon_{eff}\varepsilon_{meta}}{\varepsilon_{eff} + \varepsilon_{meta}}}, \tag{S6}$$

here, $\varepsilon_{eff} = n_{eff}^2$ represents the effective permittivity of the SW mode, and ε_{meta} represents the permittivity of the metasurface array, which can be described by the Drude-model equivalently:

$$\varepsilon_{meta}(f) = 1 - \frac{f_{meta}^2}{f^2 + i\Gamma f}, \tag{S7}$$

where f_{meta} and Γ denote the equivalent resonant frequency and damping constant of the metasurface array, respectively.

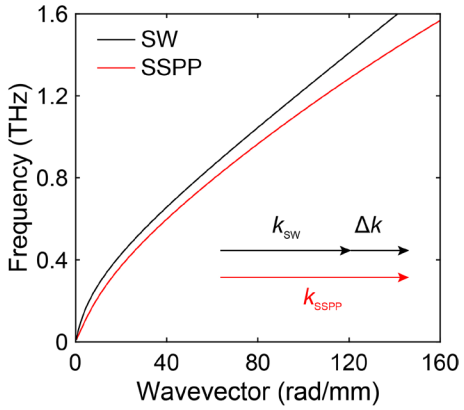

Figure S2 Dispersion curves of the SW mode and SSPP mode.

3. Settings in the simulation

The simulation calculations are performed using the commercial software Ansys Lumerical FDTD. Parameters of materials, excitation sources, and simulation settings are shown as follows. The LN is described by the Drude-Lorentz model[4]:

$$\varepsilon_{\mathrm{LN}} = \varepsilon_{\infty} + \frac{\omega_{\mathrm{TO}}^2(\varepsilon_0 - \varepsilon_{\infty})}{\omega_{\mathrm{TO}}^2 - i\omega\Gamma_{\mathrm{TO}} - \omega^2}, \tag{S8}$$

where ε_0 and ε_{∞} are the dielectric constants in low and high frequency limits, ω_{TO} and Γ_{TO} are the resonant frequency and damping rate of the lowest transverse optical phonon mode. The metasurface array is assumed to be perfect electrical conductor (PEC), because Au has a lager conductivity at the order of 10^7 S/m in the THz band. The THz source is setting as the fundamental TE_0 mode arranging from 0.2 THz to 2.0 THz.

4. Drude-Lorentz fitting for L-histidine, L-tyrosine and maltose.

The Drude-Lorentz model is widely recognized for its versatility in describing the properties of materials, where the material absorption is positively correlated to the imaginary part of the permittivity:

$$A \propto \varepsilon_{\mathrm{imag}}(f) \propto \frac{\gamma_0 f}{(f_0^2 - f^2)^2 + \gamma_0^2 f^2}, \tag{S9}$$

here, f_0 and γ_0 represent the central frequency and damping constant of fingerprint absorptions, respectively, and they are intrinsic properties of the material and are independent of the content. Besides, another parameter of the absorption curve is the

maximum at f_0, which is usually determined by the content of the analytes (see Section 5). The fitting results of the L-histidine, L-tyrosine, and maltose using Drude-Lorentz model are shown in Fig. S3. The f_0 and γ_0 are listed in Table S1.

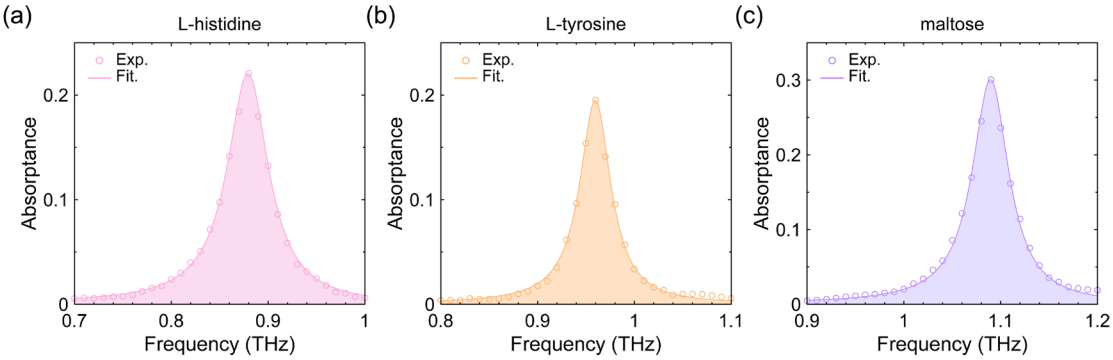

Figure S3 The fitting absorption spectra of (a) L-histidine, (b) L-Tyr, and (c) maltose using Drude-Lorentz model.

Table S1. Major absorption peak frequencies and the pertinent damping constant in the four fingerprints.

	α-lactose	L-histidine	L-tyrosine	maltose
f_0 (THz)	0.53	0.88	0.96	1.09
γ_0 (GHz)	27	52	39	47

5. Relationships between the absorptance at fingerprint frequency and the mass of biomolecules.

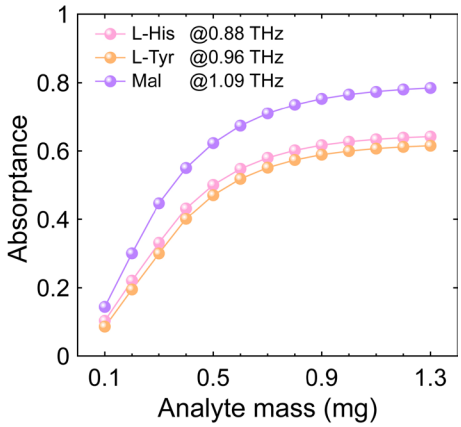

Figure S4 Relationships between the absorptance at fingerprint frequency and the mass of L-histidine, L-tyrosine, and maltose.

As depicted in Fig. S4, the absorptances of L-histidine, L-tyrosine, and maltose display a similar growing trend along with α-lactose as their mass increases, which can

be attributed to the surface localization of the THz wave by the metasensor. The differing rates of increase and saturation absorptances are resulted from variations in permittivity among the biomolecules

6. Quantitative results of biomolecular components in the mixtures.

Table S2. The measured contents of biomolecular components in the mixtures.

		Mix. 1	Mix. 2	Mix. 3	Mix. 4	Mix. 5
α-lactose	m_1 (mg)	0.204	0.204	0.198	0.197	0.203
	m_{10} (mg)	0.200	0.200	0.200	0.200	0.200
	δ	1.84%	2.15%	1.21%	1.45%	1.37%
L-histidine	m_2 (mg)			0.198		0.196
	m_{20} (mg)			0.200		0.200
	δ			1.18%		2.16%
L-tyrosine	m_3 (mg)	0.205		0.207	0.207	0.198
	m_{30} (mg)	0.200		0.200	0.200	0.200
	δ	2.57%		3.59%	3.59%	0.97%
maltose	m_4 (mg)		0.195		0.194	0.195
	m_{40} (mg)		0.200		0.200	0.200
	δ		2.49%		3.07%	2.74%

References

1 Wu, Q. *et al.* Quantitative phase contrast imaging of THz electric fields in a dielectric waveguide. *Opt. Express* **17**, 9219-9225 (2009).

2 Yang, C., Wu, Q., Xu, J., Nelson, K. A. & Werley, C. A. Experimental and theoretical analysis of THz-frequency, direction-dependent, phonon polariton modes in a subwavelength, anisotropic slab waveguide. *Opt. Express* **18**, 26351-26364 (2010).

3 Maier, S. A. Plasmonics: Fundamentals and Applications. (Springer US, 2007).

4 Xu, X. *et al.* Frequency modulation of terahertz microcavity via strong coupling with plasmonic resonators. *Opt. Express* **31**, 44375-44384 (2023).